Electrophoresis and Movements of Fluorescence Pattern After Photobleaching of Large DNA Fragments in Agarose Gels

CHI WU, ZHULUN WANG, and BENJAMIN CHU*

Chemistry Department, State University of New York at Stony Brook, New York 11794-3400

SYNOPSIS

By combining electrophoresis with movements of fluorescence pattern after photobleaching (MOFPAP), which is abbreviated as EMOFPAP, we are able to measure electrophoretic mobilities of large DNA fragments in an agarose gel within a fairly short time scale (about 10 min or even down to 1 min). The new method represents a significant improvement in experiment time when compared with the time (typically on the order of hours) required to determine the average electrophoretic mobility of large DNA fragments in agarose gels by means of either conventional gel electrophoresis or pulsed-field gel electrophoresis. In this article, we present the EMOFPAP experimental setup and consider optical conditions, including beam profile geometry and fluorescence pattern formation. A realistic formula that can explain the parameters governing the EMOFPAP method using our present optical setup has been derived. A comparison of results between experimental and computer simulation data is made, and an optimization of the EMOFPAP method is proposed.

INTRODUCTION

Fluorescence recovery after photobleaching (FRAP) has been around for at least 15 years. Modifications of this method, including photobleaching a pattern instead of a simple spot on the sample and modulation detection of the fluorescence recovery signal,[1-3] have been introduced to improve the ease with which FRAP can be applied to a variety of problems. At the present time, FRAP has already become a common technique for measuring the mobility of specific components in complex systems, especially for the measurements of lateral mobility of lipid bilayers and of proteins in cell plasma membranes and cell organelle envelopes.[4-7]

Diffusion and interaction of macromolecules in solution as well as molecular motions in the cytoplasm and nucleoplasm can also be studied using FRAP. The idea for FRAP is simple and clear. The molecular species of interest are either fluorophores or molecules labeled with a fluorophore. Mobility of the fluorophores or of the fluorophore-labeled molecules is then measured by bleaching a spot (or pattern) on the sample with an intense pulse of light. The time for the fluorescence recovery, i.e., the dissipation of the bleached pattern, is a function of the size of the bleached area and the rate of mobility of the fluorophores or the labeled molecules. The periodic pattern photobleaching technique invented by Smith and McConnell[1] makes FRAP simpler in theory and in practice. The periodic pattern can be obtained either by using a diffraction grating (such as a Ronchi ruling) or by using two coherent crossed laser beams to produce an interference pattern. Two important aspects of the periodic pattern technique are its insensitivity

CCC 0006-3525/90/030491-10 $04.00
Biopolymers, Vol. 29, 491-500 (1990)
*To whom correspondence should be addressed.

to deviation of the bleached pattern from a pure spatial sinusoid and its usefulness in detection of anisotropic diffusion in the image plane.[8]

Conventional gel electrophoresis has been a powerful analytical method for DNA separations. However, the upper limit for effective fractionation of large DNA fragments by conventional gel electrophoresis is about 20 kilobase pairs (kbp). Four years ago, Schwartz and Cantor[9] introduced a pulsed-field gel electrophoresis (PFG) technique, which pushes the upper limit of separation of DNA fragments to 2 megabase pairs (or even higher to 5 ~ 10 Mbp by modifying the geometry of the applied electric field and other considerations[10]). A more detailed review on PFG has been made by Cantor et al.[11] In PFG, one of the critical parameters is the pulse width, i.e., how long an electric field should be applied in one direction before it is switched off or applied to an opposite direction. The pulse width is one of the critical parameters responsible for limiting the DNA size separation. As the pulse width approaches the DNA reorientation time, the electrophoretic mobility changes sharply with the molecular weight. Thus, a higher resolution for DNA separation is achieved. The resolution also depends on many other parameters, such as the field strength, the gel structure, the DNA conformation and its effective charge, the geometry of the applied electric field, and the temperature. Therefore, if one could optimize those parameters, the resolution for PFG could be improved or an even higher separation limit could be achieved. It is hopeful that PFG could become one of the major analytical techniques for the human genome project because the smallest chromosome is estimated to be around 30 Mbp.[12] However, the detailed mechanisms involved in PFG have remained at a semiempirical level. Deeper explorations are needed because we want to know the relationship between the DNA mobility and its degree of stretching and deformation under an applied electric field, and how mobility and deformation are influenced by other parameters on a more microscopic scale. Orientation and stretching dynamics of large DNA fragments in agarose gels by low-field electric birefringence (TEB) have been reported by Chu et al.[13] While the low-field long-pulse-width electric birefringence measurements were able to provide information about DNA conformation dynamics related to chain orientation and stretching, the electrophoresis with movements of fluorescence pattern after photobleaching (EMOFPAP) method should provide the equally important information on DNA electrophoretic mobility almost on an instantaneous scale, i.e., over time intervals of minutes. By combining EMOFPAP with TEB, we have the means to examine the DNA dynamics in gels on a more microscopic scale.

We have successfully determined the electrophoretic mobility of λ-DNA in an agarose gel by using the newly developed EMOFPAP approach.[14] Here, we are not only able to determine the electrophoretic mobility of large DNA fragments in agarose gels in ~ 10 min or even down to 1 min instead of the order of hours in gel electrophoresis or PFG, but we also have the potential to look into the DNA electrophoretic mobility during different stages of DNA deformation in the presence of an applied electric field or immediately after the field has been turned off. We would like to point out that electrophoretic mobilities of photochromically labeled ions have already been measured by combing electrophoresis with holographic relaxation spectroscopy [HRS; also known as forced Rayleigh scattering (FRS)].[15,16] However, the molecular species of interest in HRS (or FRS) have to be photochromic or labeled with photochromic dyes whose lifetimes should be longer than the relaxation time of interest. Unfortunately, for large DNA fragments, it is not easy to find proper dyes whose lifetime are long enough so that we could attach them to large DNA fragments and measure the slow DNA electrophoretic mobility in gels. Therefore, we turned our attention to combining the gel electrophoresis with the MOFPAP method (EMOFPAP). This method has been demonstrated by using the periodic pattern fluorescence photobleaching of ethidium bromide (EB) labeled large DNA fragments in an agarose gel and subsequent observation of the electric field induced phase modulation due to the electrophoretic drift of labeled large DNA fragments. A modulation of fluorescence emission is produced as the photobleached pattern moves into and out of phase with the illumination pattern. The resulting photocurrent contains an AC component whose frequency is determined by the fringe spacing and the electrophoretic mobility of large DNA fragments. Experimentally, we can record the photocurrent and determine the drift frequency for a known fringe spacing. Therefore, the mobility of large DNA fragments can be determined. The stationary electrophoretic mobility determined by this new method[14] was in agreement with the values obtained by conventional gel electrophoresis.[17] In comparison with conventional or pulsed-field gel electrophoresis, the major distinct advantage of this new method is the very short measurement

time of a couple of minutes or less instead of hours to determine the electrophoretic mobility of large DNA fragments. The short measurement time then permits us to follow the changes in the electrophoretic mobility of large DNA fragments either after application or upon termination of an electric field, while gel electrophoresis and PFG can measure only an average electrophoretic mobility over periods of hours.

In this article, the experimental setup of EMOFPAP and a theoretical formulation based on our present optical geometry in order to properly fit the experimental data are presented. The measured results are compared with simulated data, and optimal operating conditions for the EMOFPAP experiments are discussed.

EXPERIMENTAL METHODS

Instrumentation

A schematic diagram of our EMOFPAP experimental arrangement is shown in Fig. 1. Basically, it is a typical FRAP experimental setup.[3] The only difference is that the sample holder has been modified in order to carry out electrophoresis at the same time. A 3 W argon-ion laser (Spectra-Physics 2020-03) was used for both the photobleaching (or writing) and the observation (or reading) beams. A flat optical glass plate (2) splits the incident laser beam into two beams, one (I_W) passing through the glass and the other (I_R) reflected by the glass. The subscripts R and W denote reading and writing beams, respectively. The intensity ratio of the two beams I_W/I_R is about 96 : 4. I_W and I_R are recombined by means of mirrors (1) at the second optical glass plate (2). The intensity ratio between the two recombined beams I_w and I_r is now about $1 : 10^{-3}$, since I_R undergoes a second reflection to yield a much weaker reading beam (I_r). The subscripts r and w denote the final reading and writing beams. For our experiments, the power density for I_w and I_r are 10 W/cm^2 and 10 mW/cm^2, respectively. It should be noted that we measure mainly the movements of unbleached DNA molecules that are labeled with ethidium bromide. Thus, the effect by the photochemical scission of DNA should be minimal. Computer-controlled shutters, S_1 (UniBlitze SD-10) and S_2 (UniBlitze SD-1000), are designed such that they will never open at the same time in order to protect the detector (i.e., PMT). During the bleaching process, S_1 is in the open position and S_2 is closed. During the reading process, S_1 is closed and S_2 is switched to the open position. We can use either a coarse diffraction grating [a Ronchi Ruling (3) with a frequency of 100 lines/inch] to produce a periodic pattern, as shown in Fig. 1, or use a beam splitter to split both I_w and I_r into two equal-intensity coherent laser beams and then crossing them to form a periodic interference pattern. Different fringe spacings can be achieved easily by varying the position of the first lens (L_1, a high-quality complex lens). After bleaching, S_1 is closed, which triggers S_2 to open. Fluorescence emission are collected into the PMT by the second lens (L_2), which has a large diameter (70 mm) and a short focal length (50 mm). One rejection filter (reject peak position at 488 nm) and one low-frequency-pass filter have been combined to prevent I_r (λ_0 = 488 nm) from leaking into the PMT in order to reduce the background noise. The photocurrent from the PMT (Hamamatsu R928) is amplified by an amplifier (Thorn EMI A-1). Depending on the electrophoretic mobility and fringe spacing, the amplified signal can be recorded either by an IBM-PC/AT computer through an IBM data acquisition card (12-bit resolution) or by a multichannel recorder (Biomation 8100). The timing of the applied electric field and of the EMOFPAP measurement are adjustable and controlled by the same IBM PC/AT computer.

Sample Preparation

Monodisperse λ-DNA (size = 48.5 kbp) was purchased from New England Biolabs. The stock solution, which was stored at $\simeq -20$°C, contained 500 μg/mL DNA in 10 m*M* Tris buffer (pH 8.0) and 1 m*M* EDTA. The ultrapure electrophoresis grade agarose powder with low electroendosmosis was purchased from Bethesda Research Laboratories. The DNA molecules were labeled with a trace amount of EB, i.e. ~ 0.5% of base pairs per each DNA molecule were stained with EB molecules. For the DNA–EB/agarose gel solution, we first prepared the agarose gel solution and kept it within the temperature range of 55 ~ 60°C for equilibration. Then, the DNA–EB solution was mixed with the gel solution at about 35°C (very near but above the gelation temperature), making sure that the large DNA fragments did not remain at high temperatures for any extended period of time. The well mixed DNA–EB/agarose gel solution was then pipetted at very low shear rates into the sample cell (35 × 6 × 0.6 mm). The final DNA and agarose gel concentrations were about 15 μg/mL and 0.2%, respectively. The details of sample preparation have been described elsewhere.[14]

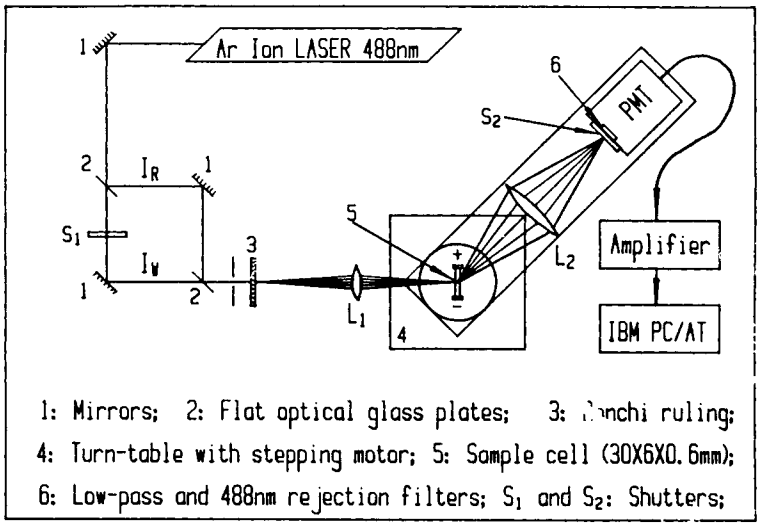

Figure 1. A schematic diagram of EFRAP experimental setup.

RESULTS AND DISCUSSION

Ideally, when we use a Ronchi ruling as a photobleaching mask to generate periodic writing (I_w) and reading (I_r) beams, both I_w and I_r should be step functions and have the following forms:

$$I_w(x) = I_{i,w} f(x) \tag{1}$$

and

$$I_r(x) = I_{i,r} f(x) \tag{2}$$

where $I_{i,w}$ and $I_{i,r}$ are the initial intensity of I_w and I_r, respectively, and $f(x)$ is a unit-amplitude square wave (jumping between 1 and 0) with period L, which can be written using the Fourier series with $K = 2\pi \sin(\theta)/L$

$$f(x) = \frac{1}{2} + \frac{2}{\pi} \sum_{n=1}^{\infty} \frac{\sin(2n-1)Kx}{2n-1} \tag{3}$$

where θ is the angle between the incident light beam and sample plane, which is usually set at 90°. The distribution of fluorescence in the specimen immediately after photobleaching can be described by the function

$$C(x,0) = C_0 - \gamma I_w(x) = C_0 - \Delta C f(x) \tag{4}$$

where γ is a constant representing the bleached fluorescence concentration per unit incident laser light intensity. C_0 and ΔC ($= \gamma I_{i,w}$ and $0 \le \Delta C \le C_0$) are the initial fluorescence concentration before photobleaching and the bleached fluorescence concentration, respectively.

If we assume that the particles making up this distribution diffuse randomly and that the rotational diffusion of the particles can be ignored, each spatial frequency component of $C(x,0)$ decays exponentially and has a characteristic rate. At time t after photobleaching, $C(x,t)$ can be expressed as

$$C(x,t) = C_0 - \Delta C g(x,t) \tag{5}$$

with

$$g(x,t) = \frac{1}{2} + \frac{2}{\pi} \sum_{n=1}^{\infty} \exp\left[-DK^2(2n-1)^2 t\right] \times \frac{\sin[(2n-1)Kx]}{2n-1} \tag{6}$$

where D is the translational diffusion constant. In the presence of the electrophoresis process, the whole photobleached periodic pattern moves spatially on top of the diffusion process. By considering both processes, we can write $C(x,t)$ as

$$C(x,t) = C_0 - \Delta C g(x - vt, vt) \tag{7}$$

with

$$g(x - vt, vt) = \frac{1}{2} + \frac{2}{\pi} \sum_{n=1}^{\infty} \exp\left[-(D/v)K^2(2n-1)^2 vt\right] \times \frac{\sin[(2n-1)K(x-vt)]}{2n-1} \tag{8}$$

where v is the speed of the moving photobleached periodic pattern in the x direction, and can be related to the electrophoretic mobility (μ) and the applied electric field (E) by $\mu = v/E$.

The detector photocurrent $F(t)$ is proportional to the fluorescence emission per spatial period. For the moving fluorescence pattern, we cannot normalize the intensity by L as described by Lanni and Ware.[2] Instead, we use an unnormalized form because we want to compare Eq. (9) with experimental results based on our present optical geometry. Then, we write

$$F(t) = \alpha \int_0^L I_r(x) C(x, t)\, dx$$

$$= \frac{1}{2}\alpha L I_{i,r}\left(C_0 - \frac{\Delta C}{2}\right)$$

$$- \frac{2}{\pi^2}\alpha L I_{i,r}\Delta C \sum_{n=1}^{\infty} \frac{1}{(2n-1)^2}$$

$$\times \exp\left[-DK^2(2n-1)^2 t\right]$$

$$\times \cos\left[(2n-1)Kvt\right] \qquad (9)$$

where α is a proportional constant. Equation (9) has a dc component and a set of decaying AC components, each of which has its own characteristic decay constant $\{\tau_{2n-1} = 1/[DK^2(2n-1)^2]\}$ and modulation frequency ($f_{2n-1} = (2n-1)Kv/(2\pi)$). The cross terms between different spatial frequencies in the photobleached pattern $[C(x, t)]$ and in the illumination pattern $[I_r(t)]$ make no contribution to $F(t)$ because they are orthogonal functions under spatial integration. The first few oscillating terms dominate contributions to $F(t)$ because, in addition to the exponential damping term, the prefactor $[1/(2n-1)^2]$ inside the sum decreases very fast with increasing n. Experimentally, by measuring the basic oscillating frequency $[f_1 = (Kv/2\pi) = v/L]$ in $F(t)$, we can calculate v for a known fringe spacing L. Four calculated curves from Eq. (9) using different ratios of D/v (ranging from 0.0001 to 0.01) are shown in Fig. 2, where $L = 0.25$ and $\Delta C = C_0 = 1$, so that $F(t)$ started at zero and the time t was rescaled to vt by simply multiplying t with v. In Fig. 2, we note that it is very difficult to obtain the electrophoretic mobility if $D/v > 0.01$.

Unfortunately, the real experimental data are not expected to follow the above idealized theory. The open triangles in Fig. 3 show real experimental

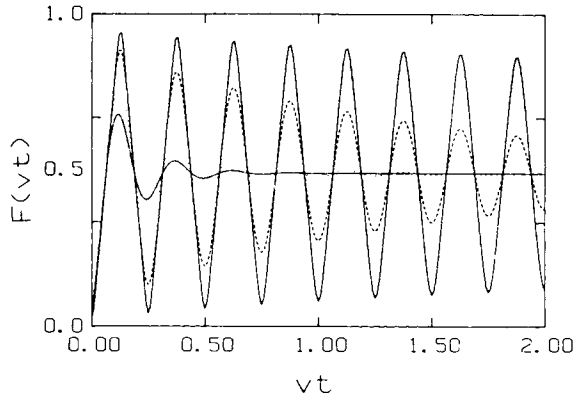

Figure 2. Calculated $F(vt)$ with different values of D/v vs vt by using Eq. (9), where we assume that $C_0 = 1$, $r = 1$, $\Delta C = 1$, $I_{0,r} = 1$, $\alpha = 1$, and $L = 0.25$. Solid line for $D/v = 10^{-4}$, dashed line for $D/v = 10^{-3}$, dotted line for $D/v = 5 \times 10^{-3}$, and broken line for $D/v = 10^{-2}$.

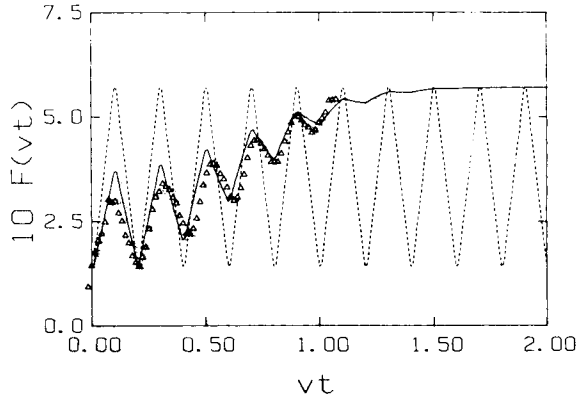

Figure 3. Comparison of calculated results from Eq. (9) (dashed line) and Eq. (23) (solid line) with real experimental data (open triangles). The experimental conditions have been rescaled with $C_0 = 1$, $r = 1$, $\Delta C = 1$, $I_{0,r} = 1$, $\alpha = 1$, $L = 0.2$, and $D/v = 0$. λ-DNA has 48.5 kbp. Agarose gel concentration is 0.2%. The electric field strength E is 2.9 V/cm. Buffer solution is made of 0.3 mM Tris buffer plus 0.03 mM EDTA. The stationary mobility μ is 7.3×10^{-5} cm^2/s-V.

data points. In Fig. 3, experimental conditions have been rescaled for comparison, i.e., $r = 1$, $C_0 = 1$, $L = 0.2$, and $D/v = 0$, because the translational diffusion of large DNA fragment in agarose gels is much smaller than the electrophoretic mobility. For comparison, we also plotted a calculated curve (dashed line) in Fig. 3 by using Eq. (9) with the same rescaled experimental conditions. The difference is so great that we have to search for a further explanation. In fact, the following conditions have

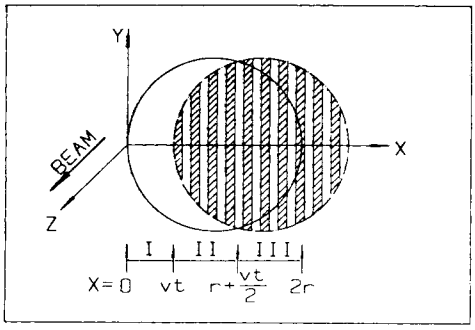

Figure 4. Schematic depiction for three parts of the integrations in Eq. (15) for the bleached pattern at time t, where we rescale the time with v.

not been taken into account in the idealized theory. (a) Both the illumination pattern and the photobleached pattern are not one-dimensional objects. (b) The laser beam intensity is not uniform spatially, but has a Gaussian profile. (c) Both the illumination pattern and the photobleached pattern have a finite size. (d) Both I_w and I_r have constant background intensity $I_{B,w}$ and $I_{B,r}$, respectively, i.e., the illumination (or the photobleached) pattern does not have a perfect "bright" and "dark" periodic pattern. Therefore, for a more realistic comparison of EMOFPAP experimental data with theory, we have to include at least the above four conditions into the theoretical consideration. In the following discussion, we present a more realistic approach for the EMOFPAP experiment and explore some experimental optimization conditions.

If we let (1) both I_w and I_r beams be along the z direction and the applied electric field be in the x direction, and approximate (2) the cross section of the laser beam to be a perfect circle, the boundary of the circle with center located at $(r,0)$ can be expressed as $y(x) = \pm[r^2 - (r-x)^2]^{1/2}$, where r is the radius of the beam cross section and $0 \le x \le 2r$ (cf. Fig. 4). (3) The beam has a Gaussian profile, which can be written as $G(x) = \exp\{-[(x/r) - 1]^2/(2\sigma^2)\}$ with the constant σ^2, defined by $\int(x - \bar{x})^2 G(x)\,dx$). Based on the above conditions, the photobleaching and illumination patterns, I_w and I_r, within the circle of $y(x) = [r^2 - (r-x)^2]^{1/2}$, whose center is located at $(r,0)$, can be written as

$$I_w(x) = I_{B,w} + I_{0,w} f(x) G(x) \tag{10}$$

and

$$I_r(x) = I_{B,r} + I_{0,r} f(x) G(x) \tag{11}$$

where $I_{B,w} + I_{0,w} = I_{i,w}$ and $I_{B,r} + I_{0,r} = I_{i,r}$. We have to keep in mind that outside the circle, there is no laser light at all, i.e., $I_w(x > 2r) = 0$ and $I_r(x > 2r) = 0$. The ratios of $I_{0,r}/I_{B,r}$ and $I_{0,w}/I_{B,w}$ actually determine the contrast of the photobleaching and illumination beam patterns. Corresponding to the change in $I_w(x)$, $C(x,0)$ should also consist of two parts. Within the illumination area, $C(x,0)$ has the form

$$\begin{aligned} C(x,0) &= C_0 - \gamma[I_{B,w} + I_{0,w} f(x) G(x)] \\ &= C_0 - C_B - \Delta C f(x) G(x) \end{aligned} \tag{12}$$

where $C_B (= \gamma I_{B,w})$ is the photobleached fluorescence concentration produced by the constant background in $I_w(x)$. Outside the illumination area, the fluorescence concentration remains at C_0. The ratio $\Delta C/C_B$ actually determines the extent of photobleaching. At time t, the whole photobleached pattern moves a distance of vt along the x direction. Within the circle, $y(x) = \{r^2 - [r - (x - vt)]^2\}^{1/2}$, where the center of the circle has moved to $x = r + vt$, $C(x,t)$ can be expressed as

$$\begin{aligned} &C(x - vt, vt) = C_0 - C_B - \Delta C g(x - vt, vt) \\ &G(x - vt), 0 \le vt \le 2r \end{aligned} \tag{13}$$

while outside the circle, $C(x,t)$ remains at C_0. The detector photocurrent now is the total fluorescence emission from the illumination area, i.e.,

$$F(t) = \alpha \int_0^{2r} C(x,t) I_r(x) y(x)\,dx \tag{14}$$

where the function $y(x)$ is used for limiting the integration within the illumination area. In order to perform this integration, Eq. (14) has to be divided into three parts, which are schematically shown in Fig. 4,

$$\begin{aligned} F(t) = \alpha &\int_0^{vt} C(x,t) I_r(x) y(x)\,dx \\ &\text{Part I} \\ &+ \alpha \int_{vt}^{r+vt/2} C(x,t) I_r(x) y(x)\,dx \\ &\text{Part II} \\ &+ \alpha \int_{r+vt/2}^{2r} C(x,t) I_r(x) y(x)\,dx \\ &\text{Part III} \end{aligned} \tag{15}$$

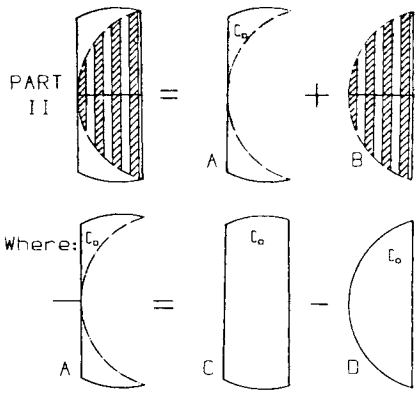

Figure 5. Schematic depiction for the integration of Part II in Eq. (15).

For Part I, $C(x, t) = C_0$, it can be integrated and written as

$$\text{Part I} = \alpha \int_0^{vt} C_0 I_r(x) y(x)\, dx \qquad (16)$$

For Part III, $C(x, t) = C(x - vt, vt)$, it can also be integrated and written as

$$\text{Part III} = \alpha \int_{r-vt/2}^{2r} C(x - vt, vt) I_r(x) y(x)\, dx \qquad (17)$$

$$= \alpha \int_{r+vt/2}^{2r} [C_0 - C_B - \Delta C g(x - vt, vt) \times G(x - vt)]\, I_r(x) y(x)\, dx \qquad (18)$$

The only difficult one is Part II. After carefully examining the Part II in Fig. 4, we find that Part II can be considered as a combination of another three small parts and graphically expressed in Fig. 5. It is clear that

$$\text{Part II} = \text{A} + \text{B} = \text{C} - \text{D} + \text{B} \qquad (19)$$

because A = C − D. Inside area C and D, $C(x, t) = C_0$. The integration of C and D can be written as follows:

$$\text{Part C} = \alpha \int_{vt}^{r+vt/2} C_0 I_r(x) y(x)\, dx \qquad (20)$$

and

$$\text{Part D} = \alpha \int_{vt}^{r+vt/2} C_0 I_r(x) y(x - vt)\, dx \qquad (21)$$

where we have replaced $y(x)$ by $y(x - vt)$ because the integration is bounded by the circle of bleached pattern instead of the circle of illumination pattern. Similarly, Part B should be integrated as

$$\text{Part B} = \alpha \int_{vt}^{r+vt/2} C(x - vt, vt) I_r(x) y(x - vt)\, dx \qquad (22)$$

because $C(x, t) = C(x - vt, vt)$ inside area B. Combining Eqs. (15)-(22), we can now write $F(t)$ as

$$F(t) = \alpha \int_0^{2r} C_0 I_r(x) y(x)\, dx - \alpha \int_{r+vt/2}^{2r} [C_B + \Delta C g(x - vt, vt) \times G(x - vt)]\, I_r(x) y(x)\, dx - \alpha \int_{vt}^{r+vt/2} [C_B + \Delta C g(x - vt, vt) \times G(x - vt)]\, I_r(x) y(x - vt)\, dx \qquad (23)$$

The solid line in Fig. 3 expresses a calculated result from Eq. (23) for the same rescaled experimental conditions. The agreement of fitting between the calculated curve and experimental data is very good and exciting. It is also obvious that the modulated frequencies for the real experimental data during the initial stages are different from those at the later stages. The modulated frequencies for the real experiment gradually approach a constant value. The difference between the real experimental data and the calculated data using a constant electrophoretic mobility is understandable because there is a stretching process mixed with the electrophoresis process during the initial application of the external electric field. This difference is more clearly shown in Fig. 6 where we doubled the spacing by changing the frequency of the Ronchi ruling from 100 lines/inch to 200 lines/inch. In Fig. 6, we note that the electrophoretic mobility is slower at the initial stage. It tells us that one single constant frequency [i.e., v because $\omega = (2\pi/L)v$] in Eq. (23) cannot quite fit the real experimental data. We have to introduce a time-dependent electrophoretic mobility $\mu(t)$. Figure 7 shows a fitting result where we have chosen $\mu_{low} (= 3.02 \times 10^{-5}$ cm^2/s-V) for initial stage mobility and $\mu_{high} (= 4.54 \times 10^{-5}$ cm^2/s-V) for later stage mobility. The fitting is fairly good as shown by Fig. 7. In order to

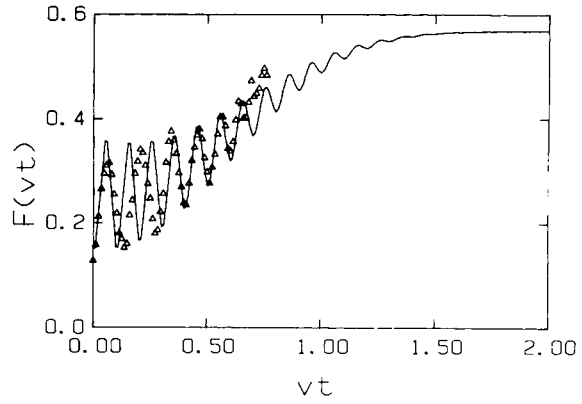

Figure 6. Comparison of calculated results from Eq. (23) (solid line) with real experimental data (open triangles). The experimental conditions have been rescaled with $C_0 = 1$, $r = 1$, $\Delta C = 1$, $I_{0,r} = 1$, $\alpha = 1$, $L = 0.1$, and $D/v = 0$. λ-DNA has 48.5 kbp. Agarose gel concentration is 0.4%. The electric field strength E is 3.5 V/cm. Buffer solution is made of 0.3 mM Tris buffer plus 0.03 mM EDTA. The stationary mobility μ is 4.54×10^{-5} cm^2/s-V.

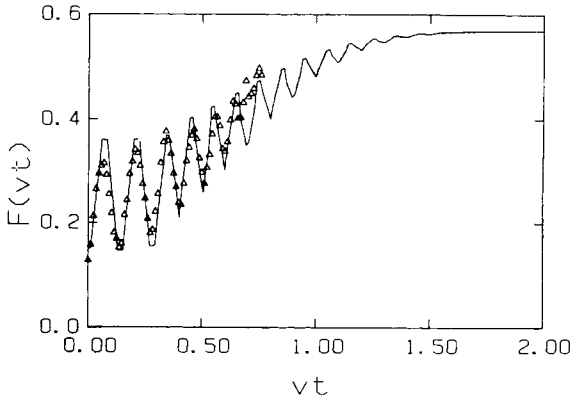

Figure 7. Comparison of calculated results from Eq. (23) (solid line) with real experimental data (open triangles). The experimental conditions have been rescaled with $C_0 = 1$, $r = 1$, $\Delta C = 1$, $I_{0,r} = 1$, $\alpha = 1$, $L = 0.1$, and $D/v = 0$. λ-DNA has 48.5 kbp. Agarose gel concentration is 0.2%. The electric field strength E is 3.5 V/cm. Buffer solution is made of 0.3 mM Tris buffer plus 0.03 mM EDTA. The two stationary mobilities, $\mu_{low} = 3.02 \times 10^{-5}$ cm^2/s-V and $\mu_{high} = 4.54 \times 10^{-5}$ cm^2/s-V, have been chosen to fit the experimental data.

obtain a functional form for the time-dependent electrophoretic mobility $\mu(t)$, more measurements are needed and the results will be presented in a forthcoming article. We only wish to point out here that $\mu(t)$ will depend on many factors, including the agarose gel concentration, the "mesh size distribution" of the agarose gel, and the size of DNA

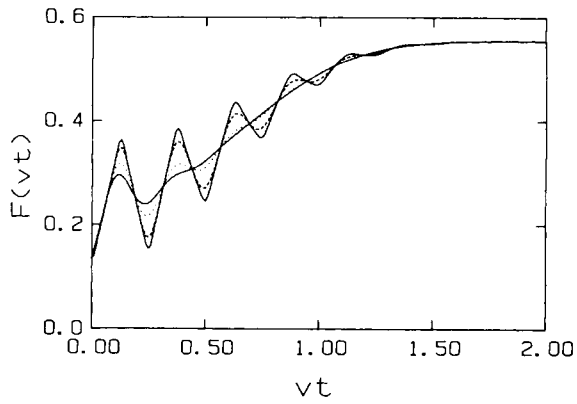

Figure 8. Calculated $F(vt)$ vs vt at different values of D/v by using Eq. (23), where $I_{B,r} = 0.2$, $I_{0,r} = 0.8$, $C_B = 0.25$, and $\Delta C = 0.75$. The remaining conditions and the line styles are the same as in Fig. 3.

fragments. It is also interesting to note that the fluorescence signal is smeared after about seven periods, probably because of the spatial inhomogeneities in the agarose gel and the small signal-to-noise ratio due to the decrease of overlap between the illumination pattern and the photobleached pattern. The measured change in mobility together with the degree of stretching should help us investigate the dynamics of DNA in agarose gels in the presence of the applied pulsed electric field on a more microscopic scale. More experiments are underway and will be discussed in subsequent articles.

With Eq. (23), we can compute $F(t)$ using a set of different experimental conditions. For simplicity, we let $C_0 = 1$, $r = 1$, $\alpha = 1$, and $L = 0.25$. Let us first consider how the self-translational diffusion of the particles of interest affects the EFRAP experiment. A set of calculated curves with different values of D/v are plotted in Fig. 8. We find that it will be very difficult to perform the EFRAP experiment when D/v is larger than $\sim 10^{-3}$, which is one order smaller than the value ($\sim 10^{-2}$) predicted by idealized theory in Fig. 2. In practice, it tells us that the larger the particle of interest and the more concentrated the gel, the easier the EFRAP experiment can be performed. For a given size particle, the requirement of the D/v ratio is satisfied either by increasing the gel concentration in order to reduce D or by increasing the electric field in order to increase v. We further consider how the contrasts of the photobleaching (I_w) and illumination (I_r) patterns affect the performance of the EFRAP experiment Fig. 9 shows three calculated $F(vt)$ vs vt curves. It tells us that the sharper

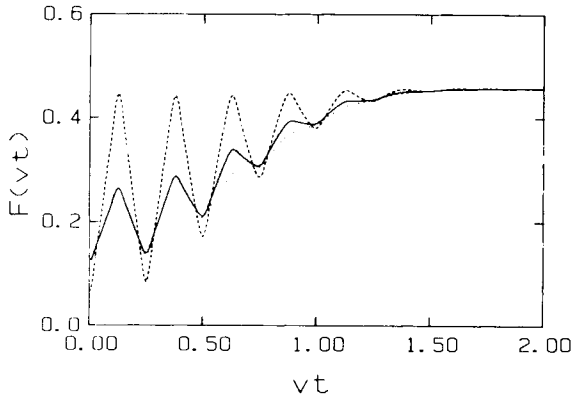

Figure 9. Calculated $F(vt)$ vs vt by using Eq. (23) with $C_0 = 1$, $r = 1$, $\alpha = 1$, $L = 0.25$, and $D/v = 10^{-4}$, but different values of $I_{B,r}$, $I_{0,r}$, C_B, and ΔC. The dashed line for $I_{B,r} = 0$, $I_{0,r} = 1$, $C_B = 0$, and $\Delta C = 1$ shows a sharp bleached and illumination pattern. The solid line for $I_{B,r} = 0.3$, $I_{0,r} = 0.7$, $C_B = 0.3$, and $\Delta C = 0.7$ shows a more realistic pattern. The dotted line for $I_{B,r} = 0.5$, $I_{0,r} = 0.5$, $C_B = 0.5$, and $\Delta C = 0.5$ shows a poor contrast, which limits the experimental measurement.

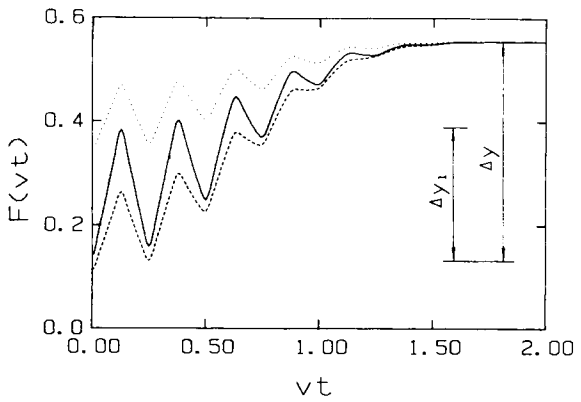

Figure 10. Calculated $F(vt)$ vs vt by using Eq. (23) with $C_0 = 1$, $r = 1$, $I_{B,r} = 0.2$, $I_{0,r} = 0.8$, $\alpha = 1$, $L = 0.25$, and $D/v = 10^{-4}$, but different values of C_B and ΔC. The dashed line for $C_B = 0.5$ and $\Delta C = 0.5$ shows an overbleached case. The dotted line for $C_B = 0.1$ and $\Delta C = 0.4$ shows an incompletely bleached case. The solid line for $C_B = 0.2$ and $\Delta C = 0.8$ shows a completely bleached case.

the contrast of the pattern, the better the signal-to-noise ratio. Experimentally, we never reach a perfect bright and dark periodic pattern because of the recombination of the diffraction pattern from the Ronchi ruling by a finite size lens, scattering from the glass walls of the sample cell, and even the sample itself. Figure 8 also tells us that the condition $I_{0,r} \gg I_{B,r}$, is an essential condition. In order to improve the experiment, we have to use a large diameter and high-quality lens in order to recombine the diffraction pattern from the Ronchi ruling, put the sample exactly at the image point of the Ronchi ruling, and make the cell surface as clean as possible. Physically, we know that the extent of photobleaching will effect the signal-to-noise ratio. Figure 10 shows three calculated $F(vt)$ vs vt curves at a different extent of photobleaching. From Fig. 9, we find that there is an optimization point about the bleaching extent where the bright part of the bleaching pattern (I_w) just bleaches out all fluorescence molecules within the pattern. This condition has to be determined experimentally because it involves many experimental conditions, such as laser light intensity, thickness of the sample, photon quantum efficiency, type of fluorescence molecules, etc. With $I_{laser} = 400$ mW, we measured the signal-to-noise ratio after different bleaching time. The results are listed in Table I where Δy and Δy_1 have been defined schematically in Fig. 10. The optimized photobleaching time is around 50 s. Finally, we discuss the method of using two coherent crossing laser beams to produce an interference pattern that serves as the photobleaching and the illumination periodic patterns. Both the photobleaching and the illumination patterns formed in this way have the sine-function form. By simply changing $f(x)$ in Eq. (23) from a step function to a sine function, we are able to calculate $F(vt)$ vs vt by crossing two coherent laser beams to form the photobleaching and the illumination periodic patterns. The dash line in Fig. 11 shows the calculated $F(vt)$ vs vt by crossing two laser beams. For comparison, we also plot a calculated $F(vt)$ vs vt curve by using the Ronchi ruling as a mask (denoted by the solid line) using exactly the same condition. The crossed beam method gives a poorer signal-to-noise ratio because the sine function is more like a "smeared" step function, i.e., having less contrast. From the above discussion, we know that the lower the contrast, the poorer signal-to-noise ratio. Experimentally, the method of crossing two coherent laser beams to

Table I Fluorescence Recovery Intensity After Different Bleaching Times

Bleaching Time (s)	Δy (V)	Δy_1	$\Delta y_1/\Delta y$ (%)
15	0.25	0.14	56
40	0.51	0.29	57
50	0.67	0.38	56
60	0.74	0.35	47

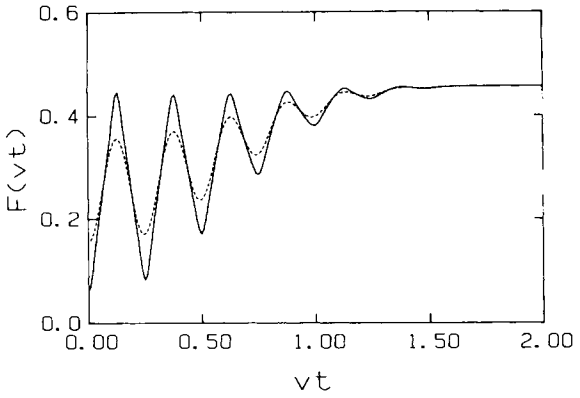

Figure 11. Calculated $F(vt)$ vs vt by using different methods to produce a periodic pattern. The solid line is by means of a Ronchi ruling. The broken line is by crossing the two laser beams. $C_0 = 1$, $r = 1$, $\alpha = 1$, $I_{B,r} = 0$, $I_{0,r} = 1$, $C_B = 0$, $\Delta C = 1$, and $D/v = 10^{-4}$.

produce the photobleaching and the illumination periodic patterns requires more time for instrument alignment. The advantage of using two crossed laser beams is being able to reach very small fringe spacings, L. Then, we are able to reduce the experimental time and possibly examine more localized DNA movements if L is smaller than the contour length of DNA fragments. In most cases, using the Ronchi ruling is better and easier for the EMOFPAP experiment.

CONCLUSION

A new method that combines electrophoresis with fluorescence recovery after photobleaching (EMOFPAP) to determine the electrophoretic mobility of large DNA fragments in agarose gels has been developed. Our theoretical approach, which takes into account the finite beam profile of both the writing and reading beams, represents the experimental results well. Optimized experimental conditions for the EMOFPAP method are discussed and predicted. EMOFPAP is able to measure the electrophoretic mobility of large DNA fragments in agarose gel within a very short time scale (about 10 min) and to provide us a new opportunity to know DNA dynamics on a more instantaneous scale.

Recent development on observation of individual EB-labeled DNA molecules undergoing gel electrophoresis with the aid of a fluorescence microscope offers another complementary approach to our technique.[18] While the fluorescence microscopic method can offer the possibility of observing electrophoretic mobility of individual DNA molecules, our method can measure the DNA electrophoretic mobility averaged over a volume element ($\sim 10^{-3}$ cm^3) that has many (e.g., $\sim 10^8$) DNA molecules. A comparison of how DNA molecules move from many individual conformations to the average value over short time periods should be particularly interesting. It should also be noted that the EB content of our DNA molecules is much lower. Furthermore, our method covers a much larger size range while the fluorescence microscope approach is limited to measurements using only very large DNA fragments.

We gratefully acknowledge support of this work by the Polymers Program of the National Science Foundation (DMR8617820).

REFERENCES

1. Smith, B. A. & McConnell, H. M. (1978) *Proc. Natl. Acad. Sci. USA* **75**, 2759–2766.
2. Lanni, F. & Ware, B. R. (1982) *Rev. Sci. Instrum.* **53**, 905–908.
3. Wahl, P. (1985) *Biophys. Chem.* **22**, 317–321.
4. Peters, R., Peters, J., Tews, K. H. & Bahr, W. (1974) *Biochim. Biophys. Acta.* **367**, 282–287.
5. Axelrod, D., Koppel, D. E., Schlessinger, J., Elson, E. & Webb, W. W. (1976) *Biophys. J.* **16**, 1055–1069.
6. Jacobson, K., Wu, E. & Poste, G. (1976) *Biochim. Biophys. Acta* **433**, 215–222.
7. Axelrod, D., Koppel, D. E., Schlessinger, J., Elson, E. & Webb, W. W. (1976) *Biophys. J.* **16**, 1315–1325.
8. Lanni, F., Taylor, D. L. & Ware, B. R. (1981) *Biophys. J.* **35**, 351–358.
9. Schwartz, D. C. & Cantor, C. R. (1984) *Cell* **37**, 67–75.
10. Carle, G. F., Frank, M. & Olson, M. V. (1986) *Science* **232**, 65–68.
11. Cantor, C. R., Smith, C. L. & Mathew, M. K. (1988) *Ann. Rev. Biophys. Chem.* **17**, 287–304.
12. Anand, R. (1986) *Trends Genet.* **2**, 278–283.
13. Chu, B., Xu, R. & Wang, Z. (1988) *Biopolymers* **27**, 2005.
14. Chu, B., Wang, Z. & Wu, C. (1989) *Biopolymers* **28**, 1491.
15. Rhee, K. W., Shibata, J., Barish, A., Gabriel, D. A. & Johnson, C. S. (1984) *J. Phys. Chem.* **88**, 3944–3946.
16. Kim, H., Chang, T. & Yu, H. (1984) *J. Phys Chem.* **88**, 3946–3949.
17. Fangman, W. L. (1978) *Nucleic Acids Res.* **5**, 653–665.
18. Smith, S. B., Aldridge, P. K. & Calls, J. B. (1989) *Science* **243**, 203–206.

Received December 27, 1988
Accepted March 9, 1989